ROYAL SOCIETY
OF CHEMISTRY

PAPER

Check for updates

Assessment of the combined radiative effects of black carbon in the atmosphere and snowpack in the Northern Hemisphere constrained by surface observations†

Tenglong Shi, [ID] [a] Yang Chen, [a] Yuxuan Xing, [a] Xiaoying Niu, [a] Dongyou Wu, [a] Jiecan Cui, [a] Yue Zhou, [a] Wei Pu [ID] [a] and Xin Wang [ID] *[ab]

In this study, the total radiative effect of black carbon (BC) in both the atmosphere and seasonal snowpack across the snow-covered area has been investigated over the Northern Hemisphere. Our results show that the annual total BC radiative effect over the snow-covered area at the top of the atmosphere varies widely from 0.93 W m^{-2} in Greenland to 5.97 W m^{-2} on the Tibetan Plateau, corresponding to contributions of snowpack BC of 10% and 70%, respectively. This highlights the important contribution of BC in snow to the assessment of the total BC radiative effect. In addition, we observed that the annual total BC radiative effect at the snow surface was generally positive, implying a dominant role of surface warming due to snowpack BC, especially in the Tibetan Plateau, where the annual total BC surface radiative effect can reach up to 4.17 W m^{-2}, indicating that BC exerts a significant influence on the snowmelt and glacier mass balance in this high-elevation region.

Environmental significance

Atmospheric black carbon (BC) aerosols can warm the atmosphere and cool the planet's surface by absorbing sunlight, whereas BC in seasonal snow can serve to warm the surface. Assessments of the BC radiative effect in snow-covered regions, however, tend to ignore the presence of BC in the snowpack, despite seasonal snow impacting >30% of the global land area and serving as a key natural water reservoir. In this study, the total radiative effect of atmospheric and snowpack BC was estimated for the snow-covered region of the Northern Hemisphere based on the snow-albedo and atmosphere radiative transfer modeling. Our results indicate that BC in snow plays a potentially significant role in local hydrology and regional climate change, particularly in High Mountain Asia.

1 Introduction

Black carbon (BC) aerosols are common byproducts of the incomplete combustion of fossil fuels, biofuels, and biomass.[1] Although they only stay in the atmosphere for periods of several days to weeks,[2,3] these particles can effectively absorb incoming solar radiation in the visible wavelength, thereby perturbing the radiative balance of the Earth system.[4–6] Furthermore, the deposition of BC on snow surfaces significantly reduces the snow albedo, thus reinforcing the melting and retreat of seasonal snowpack and glaciers.[7,8] Consequently, BC is increasingly being recognized as an important contributor to regional and global climate change.[9,10]

[a]*Key Laboratory for Semi-Arid Climate Change of the Ministry of Education, College of Atmospheric Sciences, Lanzhou University, Lanzhou 730000, China. E-mail: wxin@lzu.edu.cn*

[b]*School of Earth System Science, Tianjin University, Tianjin 300072, China*

† Electronic supplementary information (ESI) available. See https://doi.org/10.1039/d2ea00005a

The radiative effect (RE) is the difference between solar irradiance absorbed by the Earth and the longwave energy emitted to space.[11] A positive RE occurs when Earth receives more energy from the sun than it re-emits to space; this net energy gain will cause global warming.[12] Conversely, a negative RE means that Earth loses more energy to space than it receives from the sun, resulting in a cooling effect.[13] It is worth noting that the RE is distinct from the more common term "radiative forcing" (RF), which is the change in the RE from pre-industrial to present-day, thus the value of the RE is generally somewhat higher than RF and can represent RF to a certain extent.[14] Over recent decades, BC has been identified as an important contributor to global warming, second only to carbon dioxide.[10] Kopacz *et al.*[15] reported that the global annual direct radiative forcing (DRF) of atmospheric BC, due to aerosol–radiation interaction at the top of the atmosphere (TOA), is +0.36 W m^{-2}. Similarly, Wang *et al.*[16] employed a high-resolution emission inventory of BC, combined with a nested aerosol climate model, to estimate that global atmospheric BC-DRF at the TOA is 0.1–1.0 W m^{-2}. Several studies have also assessed the RE of BC in snow (*i.e.*, BC snow albedo forcing).[8,17,18] For example, Hansen

and Nazarenko[8] provided a plausible snow albedo forcing estimate of +0.3 W m^{-2} (TOA) for the Northern Hemisphere (NH), whereas Flanner et al.[17] reported a global mean annual BC/snow-surface RE of 0.007–0.12 W m^{-2}, which is considerably lower than estimates (5–10 W m^{-2}) for Northern China reported by Zhao et al.[18] Although the atmospheric BC-DRF and BC snow albedo elements have been investigated separately in these previous studies, to date, little attention has been paid to the total radiative effect of BC in both the atmosphere and snow cover concurrently.[19]

Existing uncertainties in the BC-RE are relatively large, owing to external factors including the surface albedo, water vapor, and, most notably, the presence of clouds and the vertical distribution of BC.[19–21] For instance, Haywood and Shine[22] revealed that the presence of highly reflective clouds beneath BC aerosol layers can dramatically enhance the overall RE of the atmospheric BC. Similarly, Liao and Seinfeld[23] demonstrated that a cloud layer embedded within a broad BC aerosol layer amplifies the magnitude of the RE and that this effect intensifies with increasing cloud thickness. More recently, Samset et al.[20] concluded that at least 20% of the uncertainty in modeled BC-DRF derives from the diversity of BC vertical profiles applied in twelve global aerosol models. Therefore, in order to obtain more reliable estimates of the BC-RE, these external factors must be considered in the calculation of radiation transmission and absorption.

As the most extensive component of the terrestrial cryosphere,[24] seasonal snow impacts up to 30% of Earth's land surface, and temporal variability in the snow cover is dominated by the seasonal cycle.[25] The snowpack serves as a huge water reservoir for river catchments and is especially important for sustaining plants, animals, and human populations regionally. In this study, we utilized cloud microphysical data provided by the Clouds and the Earth's Radiant Energy System (CERES), spatial and vertical characteristics of atmospheric BC obtained from MERRA-2 data, and the corrected snowpack BC data from the combination of Coupled Model Intercomparison Project Phase 6 (CMIP6) and surface observations, in conjunction with the Snow, Ice, and Aerosol Radiative (SNICAR) model and Fu–Liou radiative transfer model (RTM), to investigate the total BC-RE in the atmosphere and snow at the TOA for snow-covered areas (SCAs) of the Northern Hemisphere. Additionally, we quantify the relative contribution of BC snow albedo forcing to the total RE at the TOA. We also assess the total RE of atmospheric and snowpack BC on the surface to better understand the impact of BC on snowmelt and glacier retreat.

2 Methods

2.1 Atmospheric radiative transfer model (ARTM)

We used the Fu–Liou RTM to estimate the RE in a monthly average cloudy atmosphere both with and without a BC aerosol layer in the period 2010–2015. Developed originally by Fu and Liou[26,27] and modified subsequently by Rose and Charlock,[28] the Fu–Liou model provides the delta 2/4 stream solver for radiative transfer calculations. We employed a delta-four-stream approximation, which yields greater accuracy than the delta-

two-stream approximation, and divided the solar (0–5 μm) and infrared (5–50 μm) spectra into 6 and 12 bands, respectively. Then the correlated k-distribution method was applied to parameterize non-gray gaseous absorption by H_2O, CO_2, O_3, N_2O, and CH_4,[26] with the addition of CFCs and CO_2 in the window region.[29] In addition, Hess et al.[30] calculated the optical properties (including the respective extinction coefficients, the single scattering albedo, and the asymmetry parameter) of water clouds, ice clouds, and aerosols from the microphysical data (size distribution and the spectral refractive index), assuming that aerosol particles and cloud droplets are spherical and that cirrus cloud particles are hexagonal.[31,32] These results were embedded in the model code. The Fu–Liou RTM model has been used extensively in previous studies[33–35] and was incorporated into the Weather Research Forecast as a radiation module.[36]

2.2 Snow radiative transfer model (SRTM)

The SNICAR model has been used widely to calculate the snow spectral albedo in the fields of atmospheric and cryospheric sciences,[7,37] and also has been coupled with global climate models, such as the Community Earth System Model (CESM), which evaluates the effects of light-absorbing particles (LAPs) and snow aging on regional hydrologic cycles and climate change.[38] Since Flanner et al.[17] presented a comprehensive description of the SNICAR model, we provide only a brief summary and describe several crucial model features. SNICAR simulates radiative transfer in the snowpack via the theory of Wiscombe and Warren[39] and the two-stream multilayer radiative approximation of Toon et al.[40] It explicitly solves the vertical distributions of various snow properties, such as snow depth, snow density, and the effective snow grain radius (R_{ef}), while accounting for impurity distributions, the incident radiation type (direct or diffuse), the solar zenith angle, and the underlying land surface albedo. The optical input parameters (the extinction cross-section, single-scattering albedo, and asymmetry factor) of snow grains and impurity are calculated off-line using Mie theory and archived as look-up tables for the radiative transfer calculations. It is worth noting that the SNICAR model has recently been significantly updated with many enhancements and new features, including an adding-doubling two-stream solver, updated aerosol optical properties, and representations of non-spherical ice particles.[41] It could provide more accurate snow albedo estimates in the near-infrared (NIR) spectrum under diffuse light (cloudy) conditions. However, given that the effects of BC on the snow albedo mainly occur in the visible wavelengths, the old version of the SNICAR model used in this study is still sufficient to provide high accuracy of albedo simulations for BC-contaminated snowpack.

2.3 Calculation of the BC radiative effect

The Fu–Liou radiative transfer model provides the vertical profiles of downward (F^{down}) and upward (F^{up}) net irradiance, allowing the net irradiance (F) to be calculated from the difference between the two (i.e., $F^{down} - F^{up}$). The total BC

© 2022 The Author(s). Published by the Royal Society of Chemistry

Environ. Sci.: Atmos., 2022, **2**, 702–713 | **703**

radiative effect (RE_{tot}) is defined as the difference in net irradiance between the scenario in which BC is included in the atmospheric and snow layers ($F_{ABC,SBC}$) and the one in which BC is absent from atmospheric and snow layers ($F_{clean,clean}$):

$$RE_{tot}^{i} = F_{ABC,SBC}^{i} - F_{clean,clean}^{i} \tag{1}$$

where the superscript "i" denotes the vertical layer; we focus primarily on the results for the TOA and surface. The subscripts "ABC" and "SBC" refer to simulations that include BC in the atmosphere and snowpack, respectively, while the subscript "clean" represents cases without atmospheric or snowpack BC. Similarly, the atmospheric BC radiative effect (RE_{atmo}) and snowpack BC radiative effect (RE_{snow}) are determined using the equations:

$$RE_{atmo}^{i} = F_{ABC,SBC}^{i} - F_{clean,SBC}^{i} \tag{2}$$

$$RE_{snow}^{i} = F_{ABC,SBC}^{i} - F_{ABC,clean}^{i} \tag{3}$$

We note that the clean reference cases described here retain BC in their respective snow and atmosphere layers.

3 Results

3.1 BC in snow, and its effects on the surface albedo

Previous studies have shown that BC is the most important LAP in snow,[1,42–44] which plays a significant role in snow melting and glacier mass balance. Yet, despite numerous surface measurements of BC in snow (BC_S) having been made throughout the Northern Hemisphere in recent years,[43,45–48] important limitations remain due to discontinuities in spatial and temporal observation fields. Although the model output from CMIP6 can help to minimize this limitation, there is still significant uncertainty in previous results.[17,18] To reduce the uncertainty in the model results, we collect a large number of ground-based snowpack BC measurements in the Northern Hemisphere[42,43,45–61] and separate the Northern Hemisphere into twelve geographic regions: high-latitude North America (HNA); Greenland; western high-latitude Eurasia (WHE); eastern high-latitude Eurasia (EHE); western mid-latitude North America (WMNA); eastern mid-latitude North America (EMNA); western mid-latitude Eurasia (WME); eastern mid-latitude Eurasia (EME); western China (WC); Tibetan Plateau (TP); northeast China (NEC); and eastern China (EC). These regions are labeled in order from A to L, as shown in Fig. S1.† Then the correction factor for each region can be obtained by linear regression between the modeled and observed BC concentration and then taking the slope (Fig. S2†). Table S1† summarizes the correction factors for each region, and it should be noted that given the lack of sufficient BC measurements in some regions (F, H, and G), the correction factor for its neighboring regions is applied in these regions. Specifically, the correction factor for regions F and H follows the estimates of regions E and I, respectively, while the average of the correction factor for regions C and I instead of region G was used. Briefly, CMIP6 severely underestimates BCs in HNA, EHE, WMNA, EMNA, and TP, while it

shows good agreement with surface measurements in other regions with the correction factor ranging from 0.919 (WHE) to 1.244 (Greenland). Previous studies also revealed that the simulated BC concentrations are slightly lower than the measurements in the Arctic,[62] North America,[63] and the Tibetan Plateau,[64] which further suggests that the regional correction factors used in this study are reasonable. A more detailed description of this section can be found in the ongoing work of our colleagues.

Recognizing the significant temporal variability in the snow cover in the Northern Hemisphere,[25] Fig. S3(a–d)† shows the spatial variations in seasonal mean BC_S (corrected) for the period 2010–2014, and here the snow cover status is presented based on a combination of snow depth derived from MERRA-2 and the BC concentration derived from CMIP6. Specifically, the grid box is judged to be covered by snow when both snow depths and the BC_S concentration (CMIP6) are available (i.e., their values are greater than 0). Overall, our results exhibit substantial variability in BC_S in terms of both spatial location and seasonality. Specifically, BC_S values are higher in DJF (December, January, and February) and MAM (March, April, and May) than in JJA (June, July, and August) and SON (September, October, and November); the lower BC_S values in summer and the fall may be due to the seasonal variation in BC sources.[65–69] We also observed an apparent latitudinal dependency, with the lowest and highest BC_S values in Greenland and East Asia, respectively. Fig. S3(e)† depicts monthly changes in BC_S averaged over different regions. Generally, BC_S accumulates during the cold season and early warm season, reaching peak values in February, after which BC_S declines during the main melting season. Strong seasonal cycles are evident for EC, NEC, WC, and TP. The highest BC_S concentrations are found in EC ($\sim$600 ng g^{-1}) and NEC ($\sim$500 ng g^{-1}), where values are approximately four (two) times higher in magnitude than those in the Arctic (MNA). Similar results were also reported by Qian et al.[62]

As demonstrated above, BC_S exhibits considerable variability throughout the Northern Hemisphere. Previous model simulations have indicated that BC is the most effective at lowering the snow albedo in the ultraviolet and visible wavelengths.[56] Snow grain size is an additional key factor affecting the snow albedo. Therefore, to assess the sensitivity of the spectral snow albedo to the BC concentration and snow grain size, we simulated the spectral snow albedo using several typical BC_S contents for various Northern Hemisphere regions, with a constant R_{ef} of 200 (1000) μm for fresh (old) snow based on SNICAR model output. These values are comparable to previous observations of snow grain size at mid–high latitude sites in winter.[48,56] The model results indicate that the snow spectral albedo is substantially reduced by BC at wavelengths of <1.0 μm, with stronger reductions at higher BC concentrations and larger snow grain sizes (Fig. S4†). For example, with a fixed R_{ef} of 200 μm, the spectral albedo at 500 nm decreased by 1.8–3.3%, 5.0–11.8%, and 16.5–22.8% for typical BC concentrations of 20–50, 100–500, and 1000–2000 ng g^{-1}, respectively. In contrast, with a R_{ef} of 1000 μm, the snow

albedo decreased by 3.2–6.4%, 9.9–23.7%, and 32.4–42.9% for the same BC increments.

3.2 BC radiative effect at the TOA

It is well known that atmospheric and snowpack BC exerts a positive radiative effect at the TOA.[11] Fig. 1(a–d) show spatial variations in the seasonal total BC radiative effect (RE_{tot}^{TOA}) in the Northern Hemisphere for 2010–2014, averaged over the snow-covered surface within each grid cell. In general, spatial variations in RE_{tot}^{TOA} agree broadly with those of BC_S shown in Fig. S3,† with a larger (smaller) RE_{tot}^{TOA} for higher (lower) BC_S. However, due to the effect of solar insolation, the RE_{tot}^{TOA} presents higher values in MAM and JJA than in SON and DJF. For example, the lowest RE_{tot}^{TOA} values (<0.2 W m^{-2}) occur in the Arctic during SON and DJF, whereas the RE_{tot}^{TOA} is as much as a factor of 5–20 higher during MAM and JJA, with values of ∼1–4 W m^{-2} in Greenland, Alaska, and Western Canada. By comparison, the RE_{tot}^{TOA} for mid-latitude areas varies considerably from ∼1–4 W m^{-2} in DJF to ∼4–8 W m^{-2} in MAM.

Furthermore, to better understand the radiative effects of BC in the snow, we calculated the relative contribution of the RE of BC_S to the total RE of atmospheric and snowpack BC (RC_{snow}), as shown in Fig. 1(e–h). This pattern differs from the seasonal pattern of RF_{tot}^{TOA} because it is not affected by latitude-dependent differences in the flux of solar irradiance. Accordingly, the highest values occur over East Asia, where values of $>50\%$ imply a greater impact of BC_S than atmospheric BC on the TOA radiative effect (Fig. S5†). We suggest, therefore, that more attention should be paid to further exploring the climate effects of snowpack BC in this region. Previous studies concluded that BC plays a potentially critical role in aerosol–planetary boundary layer (PBL) interactions and the further deterioration of near-surface air pollution in megacities (i.e., the "dome effect"), particularly in the more developed regions of northern and eastern China during winter.[6,70] Our results indicate that the radiative effect of deposited BC_S in these regions can exceed that of atmospheric BC in winter. As a result, the snow darkening induced by BC_S may potentially weaken the dome effect, therefore warranting more precise quantification of this effect in the future. In contrast, the lower values ($<20\%$) observed over the Arctic, North America, and Russia indicate that atmospheric BC dominates the total BC radiative effect in these regions (Fig. S5†).

Fig. 2(a) and (b) exhibit the mean monthly RE_{tot}^{TOA} and RC_{snow}, respectively, for different regions during periods when the snow cover is present. Relatively low regionally averaged RE_{tot}^{TOA} values are observed in HNA, Greenland, WHE, EHE, WMNA, and WMNA, where the maximum values (∼2–4 W m^{-2}) are attained during May or July. These values are slightly lower than the peak RE_{tot}^{TOA} (∼4 W m^{-2}) in WME and EME in May. In contrast, the
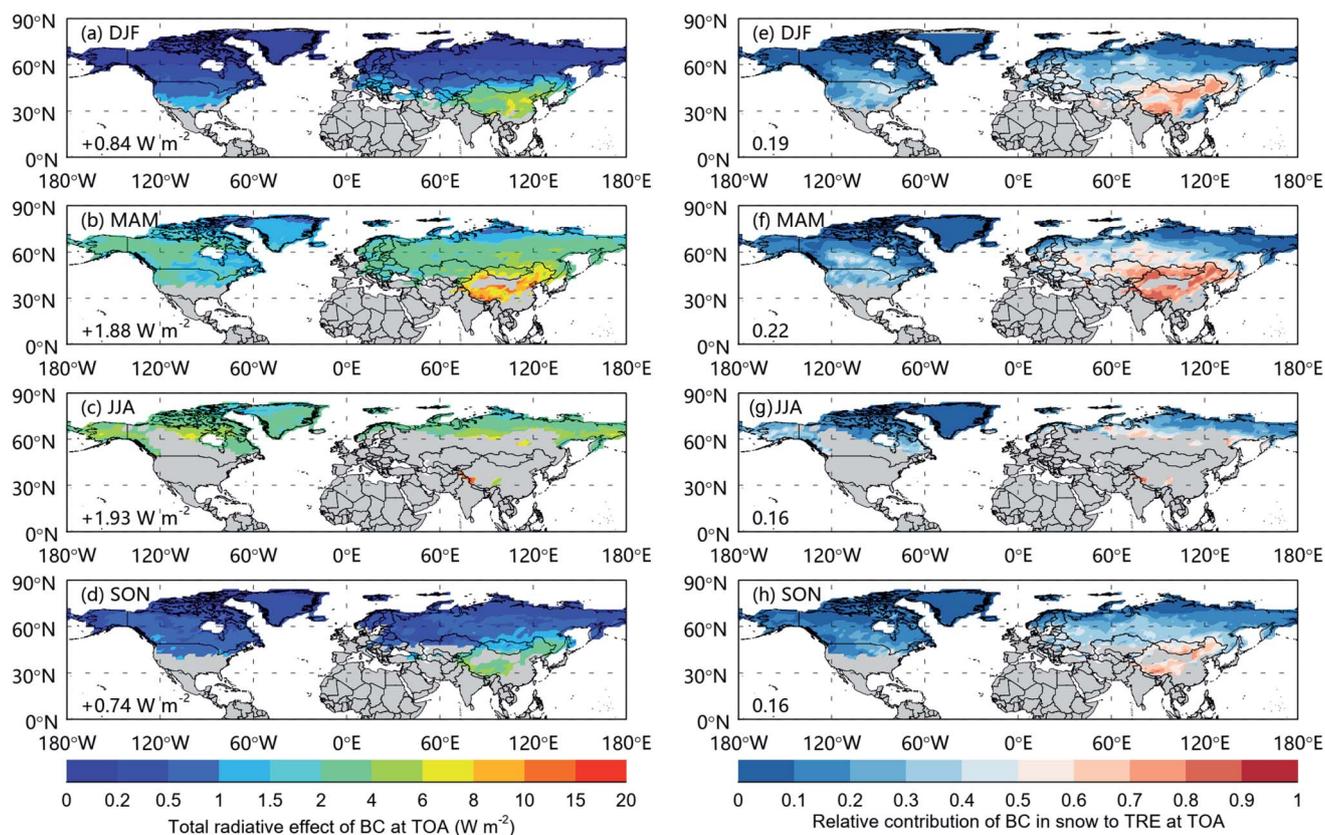

Fig. 1 Spatial distributions of the mean seasonal radiative effect of total BC in the atmosphere and snow (RE_{tot}^{TOA}) over the Northern Hemisphere for (a) DJF, (b) MAM, (c) JJA, and (d) SON in the period 2010–2014 at the TOA. Regional averages for the Northern Hemisphere are shown in the bottom left corner of each panel. (e–h) As for (a–d), but depicting the relative contribution of BC_S to the total BC radiative effect at the TOA.
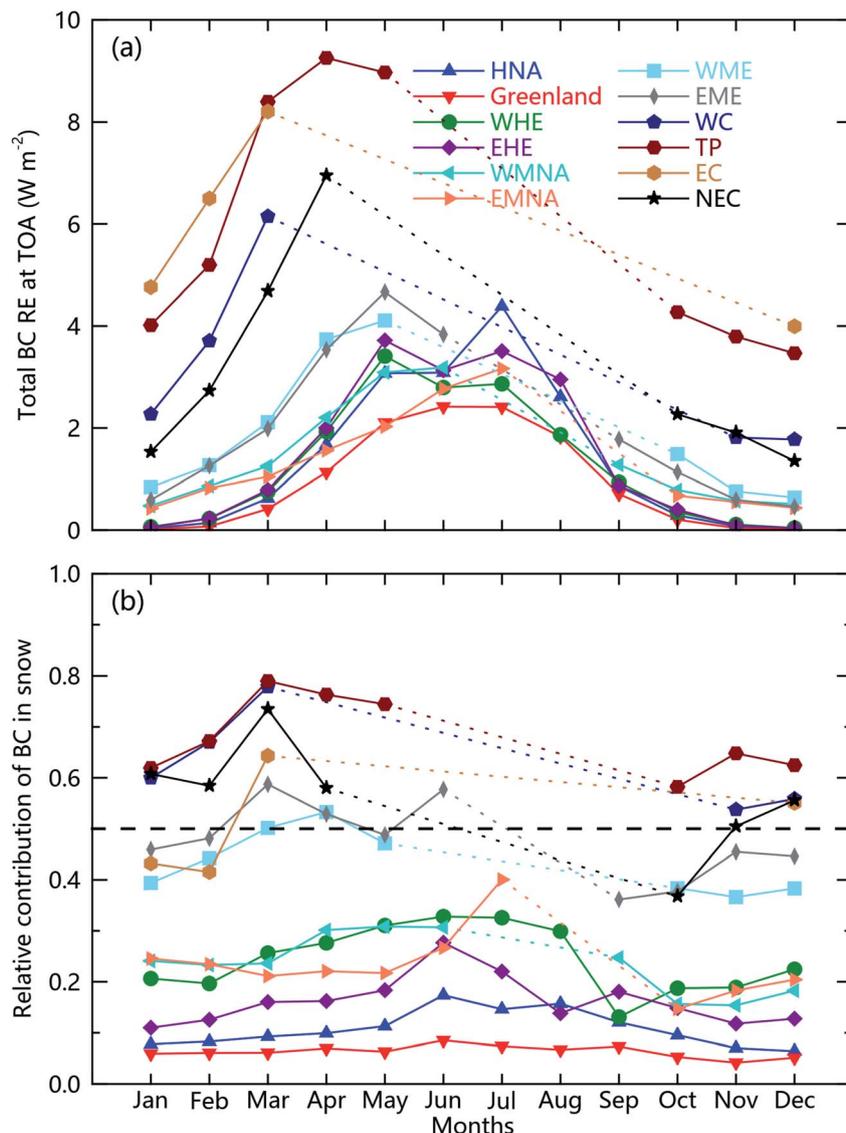
© 2022 The Author(s). Published by the Royal Society of Chemistry

Environ. Sci.: Atmos., 2022, **2**, 702–713 | **705**

Fig. 2 Mean monthly (a) total BC radiative effect (RE_{tot}^{TOA}) and (b) relative contribution of BC_S to the RE_{tot}^{TOA} at the TOA for the 12 study regions.

highest RE_{tot}^{TOA} values ($\sim$9.25 W m^{-2}) are observed over the TP during April. We note that peak RE_{tot}^{TOA} generally appears earlier with decreasing latitude, a pattern that may be attributed to that the grid box could become snow-free as snow melts, and then its radiative effect is not included in the calculation. Similarly, the regionally averaged RE_{tot}^{TOA}, peak values of RC_{snow} occur primarily in spring and summer, when the snow melts, highlighting the climatic importance of BC_S in the snowmelt period. In addition, RC_{snow} exhibits higher values ($\sim$50%) in mid-latitude regions, implying the dominant role of snowpack BC in the RE_{tot}^{TOA}. In contrast, lower RC_{snow} values (<30%) are observed in high-latitude regions, implying the dominant role of atmospheric BC in the RE_{tot}^{TOA}.

3.3 BC radiative effect at the surface

Previous studies have concluded that atmospheric and snow-pack BC can produce negative and positive radiative effects at

the surface, respectively.[8,11] However, the total surface radiative effect of atmospheric and snowpack BC, which represents the warming or cooling effect of BC on the surface, remains poorly understood. We calculated the total BC radiative effect at the surface (RE_{tot}^{Sur}); spatial distributions are illustrated in Fig. 3(a–d). During our study period, the mean seasonal RE_{tot}^{Sur} over the NH reached a minimum of approximately +0.16 W m^{-2} during SON and a maximum of +0.60 W m^{-2} in MAM. The RF_{tot}^{Sur} is generally larger in spring–summer than in autumn–winter over the same regions, a pattern that we attribute to the smaller differences between the atmospheric BC radiative effect (RE_{atmo}^{Sur}) and snow BC radiative effect (RE_{snow}^{Sur}) at the surface in the latter season (Fig. S6†). In addition, the mean seasonal RE_{tot}^{Sur} is generally positive over the NH, implying a warming effect on the surface. We note that the largest positive RE_{tot}^{Sur} occurs in the TP, where values range between $\sim$10 and 20 W m^{-2}, following the values of 5–10 W m^{-2} found in WC, EC,
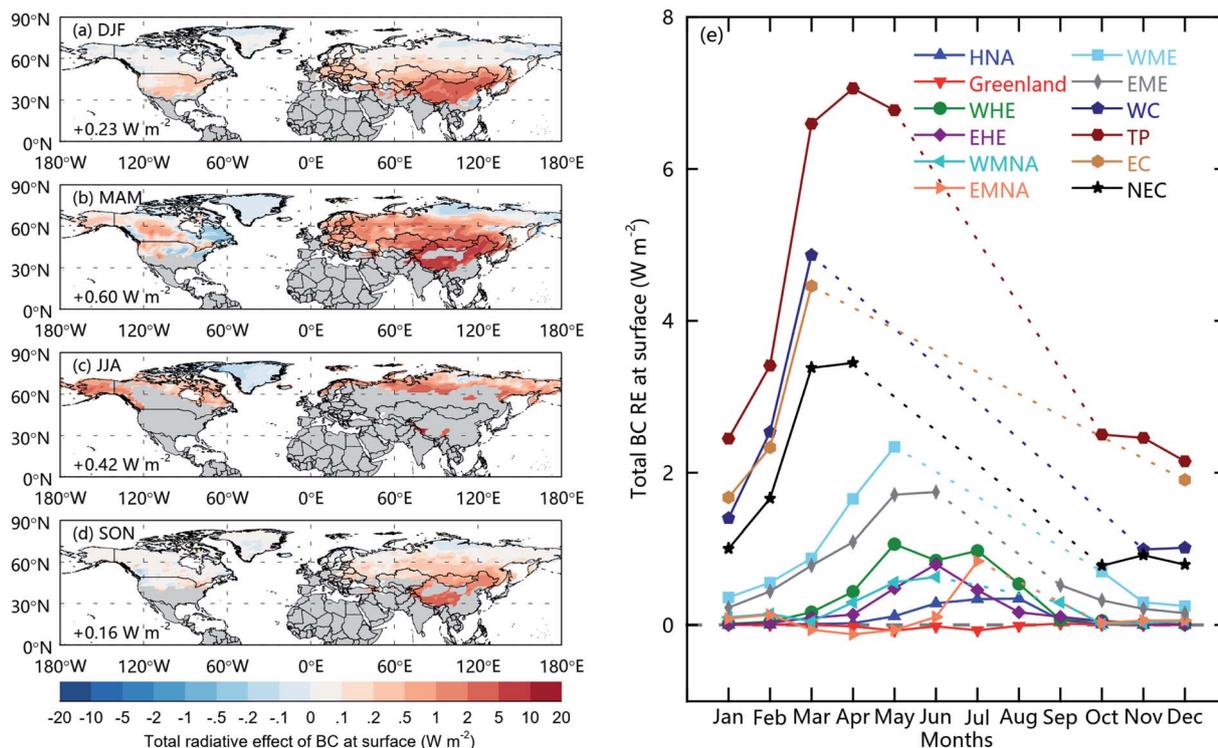
Fig. 3 (a–d) As for Fig. 1(a–d), but depicting the total BC radiative effect at the surface (RE_{tot}^{Sur}). (e) Mean monthly total BC radiative effect at the surface for each region.

and NEC. In comparison, we observed the lowest values (~-0.1 W m^{-2}) in Greenland and EMNA in MAM.

Monthly changes in RE_{tot}^{Sur}, averaged over the twelve different regions, are shown in Fig. 3(e). For almost all regions, persistent positive RE_{tot}^{Sur} values during every month imply a dominant role of surface warming due to BC$_S$ in the surface radiation budget. In addition, we found that peak values of RE_{tot}^{Sur} in mid-latitude and high-latitude regions mainly occur in spring and summer, respectively, corresponding to the timing of local snowmelt, which further emphasizes the impact of accelerated snow melting by BC and may increase the risk of occurrence of snowmelt-driven extreme events (*e.g.*, floods). Specifically, the lowest RE_{tot}^{Sur} occurs in Greenland with a value of about 0 W m^{-2}, while in other high-latitude regions, the RE_{tot}^{Sur} exhibits higher values ($\sim0-1$ W m^{-2}). With decreasing latitude, the RE_{tot}^{Sur} reaches a value of ~2 W m^{-2} in WME and EME, while in WC, EC, and NEC at similar latitudes, the RE_{tot}^{Sur} nearly doubles due to higher BC in the snowpack. In contrast, the RE_{tot}^{Sur} reaches the highest value of ~7 W m^{-2} in the TP. These results demonstrate that BC makes a greater contribution to snow and glacier ablation in regions with higher pollution, which also further underscores the importance of energy saving and emission reduction in these regions.

3.4 Regional average BC radiative effect

Fig. 4 presents the regional mean annual BC radiative effect. In general, the radiative effect of BC (total, atmosphere, and snow) spans a broad range of values, reflecting spatial and temporal variations in emissions, transportation, and deposition among

the twelve regions. At the TOA, the total BC radiative effect varies widely (0.93–5.97 W m^{-2}), with the lowest value in Greenland due to the cleanest atmosphere and snow. Similar results are observed in HNA, WHE, EHE, WMNA, and EMNA with the values of 1.05–1.32 W m^{-2}, slightly lower than the values of 1.60 W m^{-2} and 1.80 W m^{-2} found in WME and EME. The highest RE_{tot}^{TOA} occurs in East Asia and ranges from 3.38 W m^{-2} in WC to 5.97 W m^{-2} on the TP. In addition, the lowest values of RE_{snow}^{TOA} also occur in Greenland (0.07 W m^{-2}), where the radiative effect of BC in snow accounts for only 8% of the total BC RE. This value is slightly lower than that for HNA (~0.18 W m^{-2}), where BC$_S$ accounts for $\sim14\%$ of the total BC RE. The snow BC RE ($\sim0.25-0.33$ W m^{-2}) in WHE, EHE, WMNA, and EMNA, and its relative contribution ($\sim20-30\%$) to the total BC RE, exhibits similar results, while the corresponding values (~0.70 W m^{-2} and $\sim50\%$, respectively) in WME and EME are nearly double. In contrast, the snow BC RE and its relative contribution to the total BC RE in East Asia are relatively high, reflecting the impact of intense industrial pollution. For example, the highest snow BC RE occurs on the TP (3.99 W m^{-2}), due to its higher altitude and lower latitude, followed by WC (2.21 W m^{-2}) and NEC (2.12 W m^{-2}). Together, these values account for 72%, 70%, and 54% of the total BC RE, respectively, implying a significant role of snowpack BC in both local hydrology and regional climate change in East Asia. At the surface, the total BC in the atmosphere and snowpack induces a positive radiative effect over all regions, with the exception of Greenland, where the radiative effect is negative (-0.01 W m^{-2}). This indicates that BC exerts a particularly strong influence on
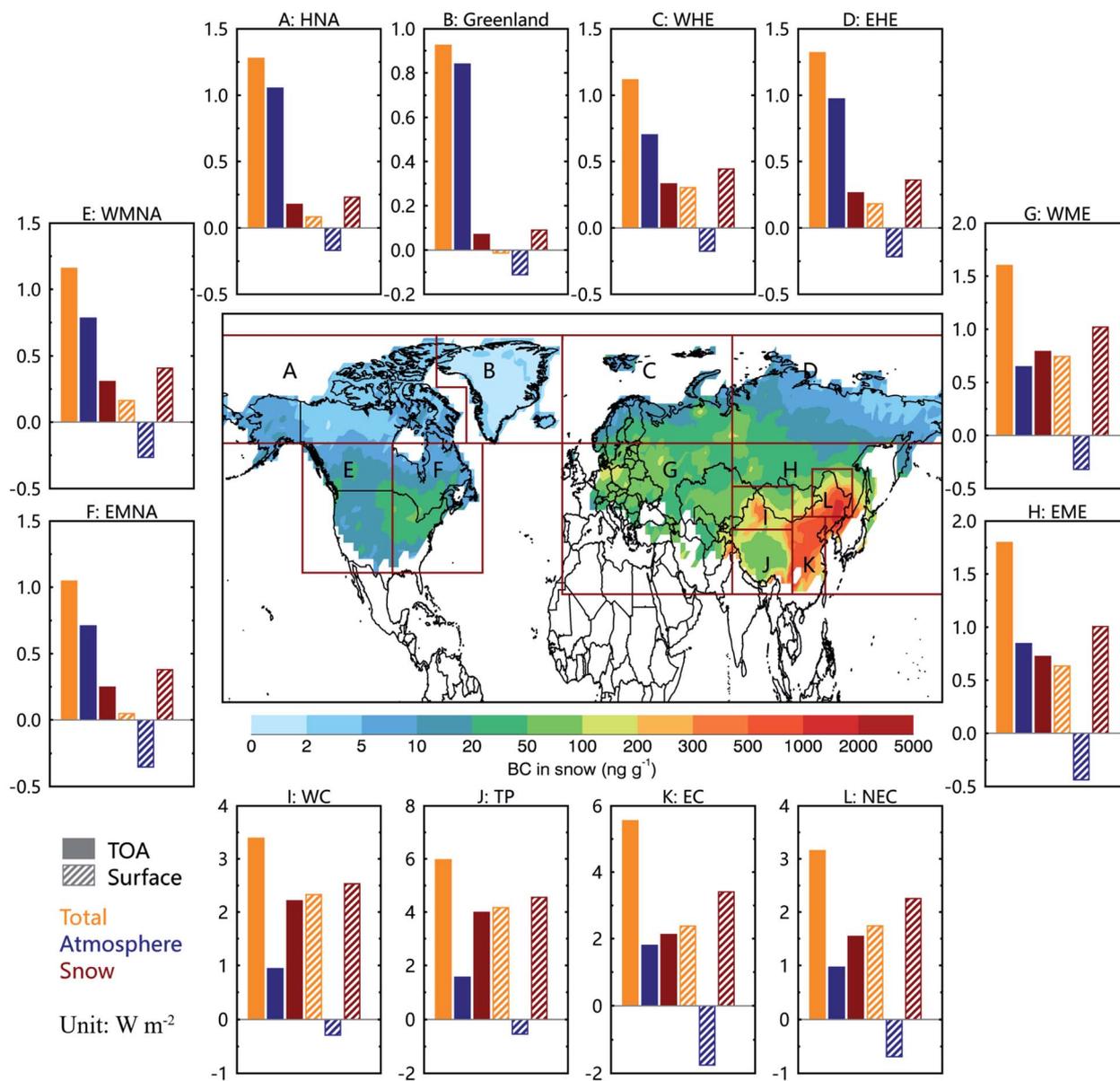
Fig. 4 Regional mean annual BC radiative effect for (a) high-latitude North America (HNA), (b) Greenland, (c) western high-latitude Eurasia (WHE), (d) eastern high-latitude Eurasia (EHE), (e) western mid-latitude North America (WMNA), (f) eastern mid-latitude North America (EMNA), (g) western mid-latitude Eurasia (WME), (h) eastern mid-latitude Eurasia (EME), (i) western China (WC), (j) Tibetan Plateau (TP), (k) eastern China (EC), and (l) northeast China (NEC).

the snowmelt and glacier mass balance in the snow-covered region. Especially in the TP, the RF_{snow}^{Sur} is up to 4.17 W m^{-2}, and similar results were reported by both Flanner *et al.*[17] and He *et al.*[71] Whereas surface dimming due to atmospheric BC dominates the surface radiation budget in Greenland. We also note that the snowpack BC RE is ~20–40% higher at the surface than at the TOA due to the influence of the atmosphere.

4 Discussion

Most previous studies quantifying the radiative effect of BC particles focused either on estimates of cooling or warming effects in the atmosphere[5,16,72] or on radiative effects of BC in the snow surface layer,[8,73] based on the model simulation or surface observations. In contrast, this study combines atmospheric radiative transfer models and snow radiative transfer models to systematically evaluate the combined radiative effects of BC in the atmosphere and snowpack in the Northern Hemisphere snow-covered region, which will further elucidate the role of BC in cryospheric climate change. Meanwhile, to reduce the uncertainty of the results, we corrected the BC concentration in snow provided by CMIP6 using a comprehensive set of ground-based snow measurements in the Northern Hemisphere over the last decade. The results show that the radiative effect of BC in snow exceeds that in the atmosphere in most regions, indicating the important climate implications of BC in snow.

However, there are still some limitations in this study; specifically, although the CMIP6 data have been corrected, the accuracy of the correction factor is debatable due to the limited snowpack BC measurements and coarse region-based division. For example, some regions cover a large variety of land-use types and topography, including desert, forest, grassland, and farm. It is unlikely that one correction factor can apply to all of the landforms. In addition, it is more noteworthy that the correction factor for some regions (*i.e.*, F, H, and G) is adopted from the values of their neighboring regions, which could result in substantial uncertainty in underlying the imperative of performing snow large-scale field experiments in these regions. Therefore, besides this investigation, we still appeal for more snowfield surveys performed to further validate and constrain the climate model simulations. Given that lower and higher correction factors would underestimate and overestimate the RE of BC in snowpack, respectively, we will collect more ground-based measurements and combine the deep learning model to give a more reliable correction factor with spatial and temporal variability in future work.

We note that the snow albedo is simulated by assuming BC external mixed with spherical snow grains in this study. Recent studies found that snow nonsphericity can interact with BC–snow mixing, which leads to 20–40% lower BC-induced albedo reductions for nonspherical snow shapes than snow spheres,[37,41,74,75] whereas BC-snow internal mixing may enhance snow albedo reduction by 30–90% relative to external mixing.[37,76] Similarly, snow grain size/growth during snow aging can also increase snow albedo reduction.[37] All these factors have remarkable impacts on the assessment of the BC radiative effect of snow due to the changes of snow albedo reduction.

It is well known that the optical parameters of BC particles are substantially influenced by their microphysical properties, *e.g.*, geometry and size distribution.[77] Many studies revealed that BC aggregates can fold up from freshly exhausted chain-like clusters into more spherical ones during the aging processes, and the aging agglomeration of BC will decrease the mass absorption coefficients (MAC) with more compact morphology and larger size.[77,78] Meanwhile, BC might also be coated with water vapor or other nucleating byproducts (*e.g.* sulphate and organic carbon) during the aging processes, which could result in higher MAC relative to uncoated BC aggregates.[79,80] Recently, more and more sophisticated geometric models have been developed to evaluate the optical properties of these nonspherical and coated BC particles, including the discrete dipole approximation (DDA),[81,82] T-matrix,[83,84] Rayleigh–Debye–Gans,[85] and geometric-optics surface-wave (GOS) approach.[86,87] However, the optical properties of BC in most radiative transfer models are still derived from Mie theory by assuming spherical aggregates. Therefore, both rigorous modeling and extensive measurements of BC size and morphology in the atmosphere and snow will be needed in further studies to reduce the uncertainty in the assessment of the BC radiative effect due to their microphysical properties. In addition, the calculations of the BC radiative effect do not includ other aerosol components in the atmosphere or snow, which may overestimate the results. Also, the main drivers (*e.g.*,

black carbon concentration in the atmosphere and snowpack, solar radiation intensity, and atmospheric conditions) of the spatiotemporal features of BC radiative effects in the atmosphere and snowpack and their respective contributions are not clear, and we will try to solve this issue in future work.

5 Conclusion

We used the SNICAR model, in conjunction with the Fu–Liou radiative transfer model, to estimate the total/atmospheric/snow BC radiative effect for the snow-covered regions of the Northern Hemisphere at both the surface and TOA. We also assessed the combined impact of vertical atmospheric BC profiles and cloud microphysical properties to reduce the magnitude of uncertainties in BC radiative effect estimates. Our results revealed a considerable degree of spatiotemporal variability in the BC radiative effect and highlighted the climatic importance of snowpack BC, particularly during the spring–summer season. At the TOA, the annual snowpack BC radiative effect varied widely, ranging from 0.07 W m^{-2} in Greenland to 3.99 W m^{-2} on the Tibetan Plateau, corresponding to 8% and 72% of the total BC radiative effect in these regions, respectively. This outcome underscores the importance of regional snowpack BC for assessments of the total BC radiative effect. At the surface, the annual snowpack BC radiative effect ranged from 0.09 to 4.56 W m^{-2}. These values are slightly higher than those at the TOA, reflecting the attenuating influence of the atmosphere. However, surface warming due to snowpack BC may ultimately dominate the surface radiation budget. Our findings indicate that the annual total BC radiative effect was positive in almost all regions and reaches the highest value in the Tibetan Plateau. These results suggest that snowpack BC plays a particularly significant role in the local hydrology and climate change of snow-covered regions, especially in High Mountain Asia.

Data availability statement

MERRA-2 Reanalysis data are available at **https://disc.gsfc.nasa.gov** (last access: 12 Jan 2022). CMIP6 data are available at **https://esgf-node.llnl.gov/search/cmip6/**(last access: 12 Jan 2022). CERES data are available at **https://ceres.larc.nasa.gov/data/**(last access: 12 Jan 2022). The SNICAR code can be obtained from **http://snow.engin.umich.edu/**(last access: 12 Jan 2022), while the source code of the Fu–Liou radiative transfer model is available *via* a Zenodo archive (**https://doi.org/10.5281/zenodo.5039613**, last access: 12 Jan 2022).

Conflicts of interest

The authors declare that they have no conflict of interest.

Acknowledgements

© 2022 The Author(s). Published by the Royal Society of Chemistry

Environ. Sci.: Atmos., 2022, **2**, 702–713 | **709**

References

1 T. C. Bond, S. J. Doherty, D. W. Fahey, P. M. Forster, T. Berntsen, B. J. DeAngelo, M. G. Flanner, S. Ghan, B. Karcher, D. Koch, S. Kinne, Y. Kondo, P. K. Quinn, M. C. Sarofim, M. G. Schultz, M. Schulz, C. Venkataraman, H. Zhang, S. Zhang, N. Bellouin, S. K. Guttikunda, P. K. Hopke, M. Z. Jacobson, J. W. Kaiser, Z. Klimont, U. Lohmann, J. P. Schwarz, D. Shindell, T. Storelvmo, S. G. Warren and C. S. Zender, Bounding the role of black carbon in the climate system: A scientific assessment, *J. Geophys. Res.: Atmos.*, 2013, **118**, 5380–5552.

2 J. N. Cape, M. Coyle and P. Dumitrean, The atmospheric lifetime of black carbon, *Atmos. Environ.*, 2012, **59**, 256–263.

3 D. Liu, C. He, J. P. Schwarz and X. Wang, Lifecycle of light-absorbing carbonaceous aerosols in the atmosphere, *npj Clim. Atmos. Sci.*, 2020, **3**, 40.

4 R. K. Chakrabarty, M. A. Garro, E. M. Wilcox and H. Moosmuller, Strong radiative heating due to wintertime black carbon aerosols in the Brahmaputra River Valley, *Geophys. Res. Lett.*, 2012, **39**, L09804.

5 S. H. Chung and J. H. Seinfeld, Climate response of direct radiative forcing of anthropogenic black carbon, *J. Geophys. Res.: Atmos.*, 2005, **110**, D11102.

6 A. J. Ding, X. Huang, W. Nie, J. N. Sun, V. M. Kerminen, T. Petaja, H. Su, Y. F. Cheng, X. Q. Yang, M. H. Wang, X. G. Chi, J. P. Wang, A. Virkkula, W. D. Guo, J. Yuan, S. Y. Wang, R. J. Zhang, Y. F. Wu, Y. Song, T. Zhu, S. Zilitinkevich, M. Kulmala and C. B. Fu, Enhanced haze pollution by black carbon in megacities in China, *Geophys. Res. Lett.*, 2016, **43**, 2873–2879.

7 O. L. Hadley and T. W. Kirchstetter, Black-carbon reduction of snow albedo, *Nat. Clim. Change*, 2012, **2**, 437–440.

8 J. Hansen and L. Nazarenko, Soot climate forcing *via* snow and ice albedos, *Proc. Natl. Acad. Sci. U. S. A.*, 2004, **101**, 423–428.

9 B. Fu, T. Gasser, B. G. Li, S. Tao, P. Ciais, S. L. Piao, Y. Balkanski, W. Li, T. Y. Yin, L. C. Han, X. Y. Li, Y. M. Han, J. An, S. Y. Peng and J. Xu, Short-lived climate forcers have long-term climate impacts *via* the carbon-climate feedback, *Nat. Clim. Change*, 2020, **10**, 851–855.

10 D. Shindell and G. Faluvegi, Climate response to regional radiative forcing during the twentieth century, *Nat. Geosci.*, 2009, **2**, 294–300.

11 V. Ramanathan and G. Carmichael, Global and regional climate changes due to black carbon, *Nat. Geosci.*, 2008, **1**, 221–227.

12 Y. Wu, T. H. Cheng, L. J. Zheng and H. Chen, Black Carbon Radiative Forcing at TOA Decreased during Aging, *Sci. Rep.*, 2016, **6**, 38592.

13 M. V. Ramana, V. Ramanathan, Y. Feng, S. C. Yoon, S. W. Kim, G. R. Carmichael and J. J. Schauer, Warming influenced by the ratio of black carbon to sulphate and the black-carbon source, *Nat. Geosci.*, 2010, **3**, 542–545.

14 C. L. Heald, D. A. Ridley, J. H. Kroll, S. R. H. Barrett, K. E. Cady-Pereira, M. J. Alvarado and C. D. Holmes, Contrasting the direct radiative effect and direct radiative forcing of aerosols, *Atmos. Chem. Phys.*, 2014, **14**, 5513–5527.

15 M. Kopacz, D. L. Mauzerall, J. Wang, E. M. Leibensperger, D. K. Henze and K. Singh, Origin and radiative forcing of black carbon transported to the Himalayas and Tibetan Plateau, *Atmos. Chem. Phys.*, 2011, **11**, 2837–2852.

16 R. Wang, Y. Balkanski, O. Boucher, P. Ciais, G. L. Schuster, F. Chevallier, B. H. Samset, J. F. Liu, S. L. Piao, M. Valari and S. Tao, Estimation of global black carbon direct radiative forcing and its uncertainty constrained by observations, *J. Geophys. Res.: Atmos.*, 2016, **121**, 5948–5971.

17 M. G. Flanner, C. S. Zender, J. T. Randerson and P. J. Rasch, Present-day climate forcing and response from black carbon in snow, *J. Geophys. Res.: Space Phys.*, 2007, **112**, D11202.

18 C. Zhao, Z. Hu, Y. Qian, L. R. Leung, J. Huang, M. Huang, J. Jin, M. G. Flanner, R. Zhang, H. Wang, H. Yan, Z. Lu and D. G. Streets, Simulating black carbon and dust and their radiative forcing in seasonal snow: a case study over North China with field campaign measurements, *Atmos. Chem. Phys.*, 2014, **14**, 11475–11491.

19 T. Donth, E. Jäkel, A. Ehrlich, B. Heinold, J. Schacht, A. Herber, M. Zanatta and M. Wendisch, Combining atmospheric and snow radiative transfer models to assess the solar radiative effects of black carbon in the Arctic, *Atmos. Chem. Phys.*, 2020, **20**, 8139–8156.

20 B. H. Samset, G. Myhre, M. Schulz, Y. Balkanski, S. Bauer, T. K. Berntsen, H. Bian, N. Bellouin, T. Diehl, R. C. Easter, S. J. Ghan, T. Iversen, S. Kinne, A. Kirkevag, J. F. Lamarque, G. Lin, X. Liu, J. E. Penner, O. Seland, R. B. Skeie, P. Stier, T. Takemura, K. Tsigaridis and K. Zhang, Black carbon vertical profiles strongly affect its radiative forcing uncertainty, *Atmos. Chem. Phys.*, 2013, **13**, 2423–2434.

21 J. Y. Xu, J. C. Zhang, J. F. Liu, K. Yi, S. L. Xiang, X. R. Hu, Y. Q. Wang, S. Tao and G. Ban-Weiss, Influence of cloud microphysical processes on black carbon wet removal, global distributions, and radiative forcing, *Atmos. Chem. Phys.*, 2019, **19**, 1587–1603.

22 J. M. Haywood and K. P. Shine, Multi-spectral calculations of the direct radiative forcing of tropospheric sulphate and soot aerosols using a column model, *Q. J. R. Meteorol. Soc.*, 1997, **123**, 1907–1930.

23 H. Liao and J. H. Seinfeld, Effect of clouds on direct aerosol radiative forcing of climate, *J. Geophys. Res.: Atmos.*, 1998, **103**, 3781–3788.

24 C. Brutel-Vuilmet, M. Menegoz and G. Krinner, An analysis of present and future seasonal Northern Hemisphere land snow cover simulated by CMIP5 coupled climate models, *Cryosphere*, 2013, **7**, 67–80.

25 D. K. Hall, G. A. Riggs and V. V. Salomonson, Development of Methods for Mapping Global Snow Cover Using Moderate

Resolution Imaging Spectroradiometer Data, *Remote Sens. Environ.*, 1995, **54**, 127–140.

26 Q. Fu and K. N. Liou, On the Correlated k-Distribution Method for Radiative Transfer in Nonhomogeneous Atmospheres, *J. Atmos. Sci.*, 1992, **49**, 2139–2156.

27 Q. Fu and K. N. Liou, Parameterization of the Radiative Properties of Cirrus Clouds, *J. Atmos. Sci.*, 1993, **50**, 2008–2025.

28 F. Rose and T. Charlock, *New Fu–Liou Code Tested with ARM Raman Lidar and CERES in Pre-CALIPSO Exercise, Extended Abstract for 11th Conference on Atmospheric Radiation (AMS)*, Ogden, Utah, 2002, pp. 3–7.

29 D. P. Kratz and F. G. Rose, Accounting for molecular absorption within the spectral range of the CERES window channel, *J. Quant. Spectrosc. Radiat. Transfer*, 1999, **61**, 83–95.

30 M. Hess, P. Koepke and I. Schult, Optical properties of aerosols and clouds: the software package OPAC, *Bull. Am. Meteorol. Soc.*, 1998, **79**, 831–844.

31 G. A. D'Almeida, P. Koepke and E. P. Shettle, *Atmospheric Aerosols: Global Climatology and Radiative Characteristics*, A Deepak Pub, 1991.

32 I. Tegen and A. A. Lacis, Modeling of particle size distribution and its influence on the radiative properties of mineral dust aerosol, *J. Geophys. Res.: Atmos.*, 1996, **101**, 19237–19244.

33 J. Huang, Q. Fu, J. Su, Q. Tang, P. Minnis, Y. Hu, Y. Yi and Q. Zhao, Taklimakan dust aerosol radiative heating derived from CALIPSO observations using the Fu-Liou radiation model with CERES constraints, *Atmos. Chem. Phys.*, 2009, **9**, 4011–4021.

34 W. W. Lin, J. J. Dai, R. Liu, Y. H. Zhai, D. L. Yue and Q. S. Hu, Integrated assessment of health risk and climate effects of black carbon in the Pearl River Delta region, China, *Environ. Res.*, 2019, **176**, 108522.

35 J. Su, J. P. Huang, Q. Fu, P. Minnis, J. M. Ge and J. R. Bi, Estimation of Asian dust aerosol effect on cloud radiation forcing using Fu–Liou radiative model and CERES measurements, *Atmos. Chem. Phys.*, 2008, **8**, 2763–2771.

36 Y. Gu, K. N. Liou, W. Chen and H. Liao, Direct climate effect of black carbon in China and its impact on dust storms, *J. Geophys. Res.: Atmos.*, 2010, **115**, D00K14.

37 C. L. He, M. G. Flanner, F. Chen, M. Barlage, K. N. Liou, S. C. Kang, J. Ming and Y. Qian, Black carbon-induced snow albedo reduction over the Tibetan Plateau: uncertainties from snow grain shape and aerosol-snow mixing state based on an updated SNICAR model, *Atmos. Chem. Phys.*, 2018, **18**, 11507–11527.

38 D. M. Lawrence, K. W. Oleson, M. G. Flanner, C. G. Fletcher, P. J. Lawrence, S. Levis, S. C. Swenson and G. B. Bonan, The CCSM4 Land Simulation, 1850–2005: Assessment of Surface Climate and New Capabilities, *J. Clim.*, 2012, **25**, 2240–2260.

39 W. J. Wiscombe and S. G. Warren, A Model for the Spectral Albedo of Snow .1. Pure Snow, *J. Atmos. Sci.*, 1980, **37**, 2712–2733.

40 O. B. Toon, C. P. Mckay, T. P. Ackerman and K. Santhanam, Rapid Calculation of Radiative Heating Rates and Photodissociation Rates in Inhomogeneous Multiple-

Scattering Atmospheres, *J. Geophys. Res.: Atmos.*, 1989, **94**, 16287–16301.

41 M. G. Flanner, J. B. Arnheim, J. M. Cook, C. Dang, C. He, X. Huang, D. Singh, S. M. Skiles, C. A. Whicker and C. S. Zender, SNICAR-ADv3: a community tool for modeling spectral snow albedo, *Geosci. Model Dev.*, 2021, **14**, 7673–7704.

42 S. J. Doherty, S. G. Warren, T. C. Grenfell, A. D. Clarke and R. E. Brandt, Light-absorbing impurities in Arctic snow, *Atmos. Chem. Phys.*, 2010, **10**, 11647–11680.

43 X. Wang, S. J. Doherty and J. Huang, Black carbon and other light-absorbing impurities in snow across Northern China, *J. Geophys. Res.: Atmos.*, 2013, **118**, 1471–1492.

44 X. Wang, B. Xu and J. Ming, An overview of the studies on black carbon and mineral dust deposition in snow and ice cores in East Asia, *J. Meteorol. Res.*, 2014, **28**, 354–370.

45 S. J. Doherty, C. Dang, D. A. Hegg, R. D. Zhang and S. G. Warren, Black carbon and other light-absorbing particles in snow of central North America, *J. Geophys. Res.: Atmos.*, 2014, **119**, 12807–12831.

46 J. Ming, C. D. Xiao, H. Cachier, D. H. Qin, X. Qin, Z. Q. Li and J. C. Pu, Black Carbon (BC) in the snow of glaciers in west China and its potential effects on albedos, *Atmos. Res.*, 2009, **92**, 114–123.

47 W. Pu, X. Wang, H. L. Wei, Y. Zhou, J. S. Shi, Z. Y. Hu, H. C. Jin and Q. L. Chen, Properties of black carbon and other insoluble light-absorbing particles in seasonal snow of northwestern China, *Cryosphere*, 2017, **11**, 1213–1233.

48 X. Wang, W. Pu, Y. Ren, X. Zhang, X. Zhang, J. Shi, H. Jin, M. Dai and Q. Chen, Observations and model simulations of snow albedo reduction in seasonal snow due to insoluble light-absorbing particles during 2014 Chinese survey, *Atmos. Chem. Phys.*, 2017, **17**, 2279–2296.

49 S. Kaspari, T. H. Painter, M. Gysel, S. M. Skiles and M. Schwikowski, Seasonal and elevational variations of black carbon and dust in snow and ice in the Solu-Khumbu, Nepal and estimated radiative forcings, *Atmos. Chem. Phys.*, 2014, **14**, 8089–8103.

50 X. F. Li, S. C. Kang, X. B. He, B. Qu, L. Tripathee, Z. F. Jing, R. Paudyal, Y. Li, Y. L. Zhang, F. P. Yan, G. Li and C. L. Li, Light-absorbing impurities accelerate glacier melt in the Central Tibetan Plateau, *Sci. Total Environ.*, 2017, **587**, 482–490.

51 J. Ming, C. D. Xiao, F. T. Wang, Z. Q. Li and Y. M. Li, Grey Tienshan Urumqi Glacier No. 1 and light-absorbing impurities, *Environ. Sci. Pollut. Res.*, 2016, **23**, 9549–9558.

52 T. Mori, K. Goto-Azuma, Y. Kondo, Y. Ogawa-Tsukagawa, K. Miura, M. Hirabayashi, N. Oshima, M. Koike, K. Kupiainen, N. Moteki, S. Ohata, P. R. Sinha, K. Sugiura, T. Aoki, M. Schneebeli, K. Steffen, A. Sato, A. Tsushima, V. Makarov, S. Omiya, A. Sugimoto, S. Takano and N. Nagatsuka, Black Carbon and Inorganic Aerosols in Arctic Snowpack, *J. Geophys. Res.: Atmos.*, 2019, **124**, 13325–13356.

53 H. W. Niu, S. C. Kang, Y. L. Zhang, X. Y. Shi, X. F. Shi, S. J. Wang, G. Li, X. G. Yan, T. Pu and Y. Q. He, Distribution of light-absorbing impurities in snow of

© 2022 The Author(s). Published by the Royal Society of Chemistry

Environ. Sci.: Atmos., 2022, **2**, 702–713 | **711**

glacier on Mt. Yulong, southeastern Tibetan Plateau, *Atmos. Res.*, 2017, **197**, 474–484.

54 B. Qu, J. Ming, S. C. Kang, G. S. Zhang, Y. W. Li, C. D. Li, S. Y. Zhao, Z. M. Ji and J. J. Cao, The decreasing albedo of the Zhadang glacier on western Nyainqentanglha and the role of light-absorbing impurities, *Atmos. Chem. Phys.*, 2014, **14**, 11117–11128.

55 P. M. Rowe, R. R. Cordero, S. G. Warren, E. Stewart, S. J. Doherty, A. Pankow, M. Schrempf, G. Casassa, J. Carrasco, J. Pizarro, S. MacDonell, A. Damiani, F. Lambert, R. Rondanelli, N. Huneeus, F. Fernandoy and S. Neshyba, Black carbon and other light-absorbing impurities in snow in the Chilean Andes, *Sci. Rep.*, 2019, **9**, 4008.

56 T. Shi, W. Pu, Y. Zhou, J. Cui, D. Zhang and X. Wang, Albedo of Black Carbon-Contaminated Snow Across Northwestern China and the Validation With Model Simulation, *J. Geophys. Res.: Atmos.*, 2020, **125**, e2019JD032065.

57 B. Q. Xu, J. J. Cao, D. R. Joswiak, X. Q. Liu, H. B. Zhao and J. Q. He, Post-depositional enrichment of black soot in snow-pack and accelerated melting of Tibetan glaciers, *Environ. Res. Lett.*, 2012, **7**, 014022.

58 S. Yang, B. Q. Xu, J. J. Cao, C. S. Zender and M. Wang, Climate effect of black carbon aerosol in a Tibetan Plateau glacier, *Atmos. Environ.*, 2015, **111**, 71–78.

59 Y. Zhang, T. Gao, S. Kang, M. Sprenger, S. Tao, W. Du, J. Yang, F. Wang and W. Meng, Effects of black carbon and mineral dust on glacial melting on the Muz Taw glacier, Central Asia, *Sci. Total Environ.*, 2020, **740**, 140056.

60 Y. L. Zhang, S. C. Kang, Z. Y. Cong, J. Schmale, M. Sprenger, C. L. Li, W. Yang, T. G. Gao, M. Sillanpaa, X. F. Li, Y. J. Liu, P. F. Chen and X. L. Zhang, Light-absorbing impurities enhance glacier albedo reduction in the southeastern Tibetan plateau, *J. Geophys. Res.: Atmos.*, 2017, **122**, 6915–6933.

61 Y. L. Zhang, S. C. Kang, M. Sprenger, Z. Y. Cong, T. G. Gao, C. L. Li, S. Tao, X. F. Li, X. Y. Zhong, M. Xu, W. J. Meng, B. Neupane, X. Qin and M. Sillanpaa, Black carbon and mineral dust in snow cover on the Tibetan Plateau, *Cryosphere*, 2018, **12**, 413–431.

62 Y. Qian, H. L. Wang, R. D. Zhang, M. G. Flanner and P. J. Rasch, A sensitivity study on modeling black carbon in snow and its radiative forcing over the Arctic and Northern China, *Environ. Res. Lett.*, 2014, **9**, 064001.

63 C. L. Wu, X. H. Liu, Z. H. Lin, S. R. Rahimi-Esfarjani and Z. Lu, Impacts of absorbing aerosol deposition on snowpack and hydrologic cycle in the Rocky Mountain region based on variable-resolution CESM (VR-CESM) simulations, *Atmos. Chem. Phys.*, 2018, **18**, 511–533.

64 C. Sarangi, Y. Qian, K. Rittger, K. J. Bormann, Y. Liu, H. Wang, H. Wan, G. Lin and T. H. Painter, Impact of light-absorbing particles on snow albedo darkening and associated radiative forcing over high-mountain Asia: high-resolution WRF-Chem modeling and new satellite observations, *Atmos. Chem. Phys.*, 2019, **19**, 7105–7128.

65 D. A. Hegg, S. G. Warren, T. C. Grenfell, J. D. Sarah and A. D. Clarke, Sources of light-absorbing aerosol in arctic snow and their seasonal variation, *Atmos. Chem. Phys.*, 2010, **10**, 10923–10938.

66 M. M. Ruppel, S. Eckhardt, A. Pesonen, K. Mizohata, M. J. Oinonen, A. Stohl, A. Andersson, V. Jones, S. Manninen and Ö. Gustafsson, Observed and Modeled Black Carbon Deposition and Sources in the Western Russian Arctic 1800–2014, *Environ. Sci. Technol.*, 2021, **55**, 4368–4377.

67 P. Winiger, A. Andersson, S. Eckhardt, A. Stohl, I. P. Semiletov, O. V. Dudarev, A. Charkin, N. Shakhova, Z. Klimont and C. Heyes, Siberian Arctic Black Carbon Sources Constrained by Model and Observation, *Proc. Natl. Acad. Sci. U. S. A.*, 2017, **114**, E1054–E1061.

68 Y. Yang, H. L. Wang, S. J. Smith, P. L. Ma and P. J. Rasch, Source attribution of black carbon and its direct radiative forcing in China, *Atmos. Chem. Phys.*, 2017, **17**, 4319–4336.

69 R. Zhang, H. Wang, Y. Qian, P. J. Rasch, R. C. Easter, P. L. Ma, B. Singh, J. Huang and Q. Fu, Quantifying sources, transport, deposition, and radiative forcing of black carbon over the Himalayas and Tibetan Plateau, *Atmos. Chem. Phys.*, 2015, **15**, 6205–6223.

70 Z. L. Wang, X. Huang and A. J. Ding, Dome effect of black carbon and its key influencing factors: a one-dimensional modelling study, *Atmos. Chem. Phys.*, 2018, **18**, 2821–2834.

71 C. L. He, Q. B. Li, K. N. Liou, Y. Takano, Y. Gu, L. Qi, Y. H. Mao and L. R. Leung, Black carbon radiative forcing over the Tibetan Plateau, *Geophys. Res. Lett.*, 2014, **41**, 7806–7813.

72 R. Cherian, J. Quaas, M. Salzmann and L. Tomassini, Black carbon indirect radiative effects in a climate model, *Tellus B*, 2017, **69**, 1369342.

73 C. Dang, S. G. Warren, Q. Fu, S. J. Doherty, M. Sturm and J. Su, Measurements of light-absorbing particles in snow across the Arctic, North America, and China: effects on surface albedo, *J. Geophys. Res.: Atmos.*, 2017, **122**, 10149–10168.

74 C. Dang, Q. Fu and S. G. Warren, Effect of Snow Grain Shape on Snow Albedo, *J. Atmos. Sci.*, 2016, **73**, 3573–3583.

75 C. L. He, K. N. Liou, Y. Takano, F. Chen and M. Barlage, Enhanced Snow Absorption and Albedo Reduction by Dust-Snow Internal Mixing: Modeling and Parameterization, *J. Adv. Model. Earth Syst.*, 2019, **11**, 3755–3776.

76 M. G. Flanner, X. Liu, C. Zhou, J. E. Penner and C. Jiao, Enhanced solar energy absorption by internally-mixed black carbon in snow grains, *Atmos. Chem. Phys.*, 2012, **12**, 4699–4721.

77 C. He, K. N. Liou, Y. Takano, R. Zhang, M. L. Zamora, P. Yang, Q. Li and L. R. Leung, Variation of the radiative properties during black carbon aging: theoretical and experimental intercomparison, *Atmos. Chem. Phys.*, 2015, **15**, 11967–11980.

78 Y. Wang, Y. Pang, J. Huang, L. Bi, H. Che, X. Zhang and W. Li, Constructing Shapes and Mixing Structures of Black Carbon Particles With Applications to Optical Calculations, *J. Geophys. Res.: Atmos.*, 2021, **126**, e2021JD034620.

79 T. C. Bond, G. Habib and R. W. Bergstrom, Limitations in the enhancement of visible light absorption due to mixing state, *J. Geophys. Res.: Atmos.*, 2006, **111**, D20211.

80 D. T. Liu, J. Whitehead, M. R. Alfarra, E. Reyes-Villegas, D. V. Spracklen, C. L. Reddington, S. F. Kong, P. I. Williams, Y. C. Ting, S. Haslett, J. W. Taylor, M. J. Flynn, W. T. Morgan, G. McFiggans, H. Coe and J. D. Allan, Black-carbon absorption enhancement in the atmosphere determined by particle mixing state, *Nat. Geosci.*, 2017, **10**, 184–188.

81 K. Adachi, S. H. Chung and P. R. Buseck, Shapes of soot aerosol particles and implications for their effects on climate, *J. Geophys. Res.: Atmos.*, 2010, **115**, D15206.

82 B. V. Scarnato, S. Vahidinia, D. T. Richard and T. W. Kirchstetter, Effects of internal mixing and aggregate morphology on optical properties of black carbon using a discrete dipole approximation model, *Atmos. Chem. Phys.*, 2013, **13**, 5089–5101.

83 L. Liu and M. I. Mishchenko, Scattering and radiative properties of complex soot and soot-containing aggregate particles, *J. Quant. Spectrosc. Radiat. Transfer*, 2007, **106**, 262–273.

84 M. I. Mishchenko, L. Liu and D. W. Mackowski, T-matrix modeling of linear depolarization by morphologically complex soot and soot-containing aerosols, *J. Quant. Spectrosc. Radiat. Transfer*, 2013, **123**, 135–144.

85 T. L. Farias, U. O. Koylu and M. G. Carvalho, Range of validity of the Rayleigh–Debye–Gans theory for optics of fractal aggregates, *Appl. Opt.*, 1996, **35**, 6560–6567.

86 K. N. Liou, Y. Takano and P. Yang, Light absorption and scattering by aggregates: application to black carbon and snow grains, *J. Quant. Spectrosc. Radiat. Transfer*, 2011, **112**, 1581–1594.

87 Y. Takano, K. N. Liou, M. Kahnert and P. Yang, The single-scattering properties of black carbon aggregates determined from the geometric-optics surface-wave approach and the T-matrix method, *J. Quant. Spectrosc. Radiat. Transfer*, 2013, **125**, 51–56.